REPORT DOCUMENTATION PAGE

Form Approved
OMB No. 0704-0188

1. REPORT DATE (DD-MM-YYYY)	2. REPORT TYPE	3. DATES COVERED (From - To)
30-Jun-06	Final	10/1/02-1/31/06

4. TITLE AND SUBTITLE
Minority Carrier Lifetime in SiC Epilayers Growth by Halide CVD

5a. CONTRACT NUMBER
N00014-03-1-0005

5b. GRANT NUMBER
05PR00506

5c. PROGRAM ELEMENT NUMBER

6. AUTHOR(S)
SKOWRONSKI, Marek

5d. PROJECT NUMBER

5e. TASK NUMBER

5f. WORK UNIT NUMBER

7. PERFORMING ORGANIZATION NAME(S) AND ADDRESS(ES)
Carnegie Mellon University
Office of Sponsored Research
5000 Forbes Avenue
Pittsburgh PA 15213

8. PERFORMING ORGANIZATION REPORT NUMBER

9. SPONSORING/MONITORING AGENCY NAME(S) AND ADDRESS(ES)
Office of Naval Research
Regional Office Chicago
230 South Dearborn, Room 380
Chicago IL 60604-1595

10. SPONSOR/MONITOR'S ACRONYM(S)
N62880

11. SPONSORING/MONITORING AGENCY REPORT NUMBER
ONR 245

12. DISTRIBUTION AVAILABILITY STATEMENT

DISTRIBUTION STATEMENT A
Approved for Public Release
Distribution Unlimited

13. SUPPLEMENTARY NOTES

14. ABSTRACT
High purity 6H-SiC single crystals have been grown by the Halide Chemical Vapor Deposition process. Growth was performed using separate injection of silicon silicon tetrachloride and propane. The growth rates were between 100 µm/hr and 300 µm/hr. The crystals show very low concentrations of residual impurities with the main contaminants, namely nitrogen and boron, in the 10^{14} cm^{-3} range. Crystals grown under Si-rich conditions were n-type with low room temperature electron concentration in the 10^{14}-10^{15} cm^{-3} range and the 300K electron mobilities approaching 400 cm2/Vs. The resistivity of the material increased up to 10^{10} Ωcm with increasing the C/Si ratio. Electron traps density decreases with the increase of C/Si ratio. Carrier lifetimes of HCVD material correlate with deep center concentrations. Lifetimes increase with increase of C/Si ratio and growth temperature.

15. SUBJECT TERMS

16. SECURITY CLASSIFICATION OF:			17. LIMITATION OF ABSTRACT	18. NUMBER OF PAGES	19a. NAME OF RESPONSIBLE PERSON
a. REPORT	b. ABSTRACT	c. THIS PAGE			19b. TELEPONE NUMBER (Include area code)

Standard Form 298 (Rev. 8-98)
Prescribed by ANSI-Std Z39-18

Final Technical Report

Project Title: Minority Carrier Lifetimes in Halide Chemical Vapor Deposition SiC
Project #: N00014-03-01-0005
Institution: Carnegie Mellon university
PI: Marek Skowronski

20060710060

Summary

High purity 6H-SiC single crystals have been grown by the Halide Chemical Vapor Deposition (HCVD) process. Growth was performed in a vertical hot-wall reactor with the separate injection of silicon precursor (silicon tetrachloride) and carbon precursor (propane). The typical growth rates were between 100 μm/hr and 300 μm/hr. The crystals show very low concentrations of residual impurities with the main contaminants, namely nitrogen and boron, in the 10^{14} cm^{-3} range. Crystals grown under Si-rich conditions were n-type with low room temperature electron concentration in the 10^{14}-10^{15} cm^{-3} range and the room temperature electron mobilities approaching 400 cm^2/Vs. The resistivity of the material increased up to 10^{10} Ωcm with increasing the C/Si ratio. Deep levels spectra show that the electron traps density decreases with the increase of C/Si ratio. Carrier lifetimes of HCVD material were measured on variety of samples and were found to correlate well with deep center concentrations. Lifetimes increase with increase of C/Si ratio and with increase of the growth temperature. The center that appears to limit lifetimes is the electron trap located 1.0 eV below conduction band.

1. Goals

The major driving force for the development of silicon carbide-based electronic devices are the applications in power control, transmission, and conditioning. High voltage power subsystems require two types of devices: diodes and switches. For intermediate voltages between 1 and 3 kV, the optimum diode/swich combination is Schottky (SBD) and MOSFET tandem. At voltages above 3 kV, the resistive losses in Schottky barriers grow to large and SBDs should be replaced by bipolar p-i-n diodes. Similarly, at blocking voltage in excess of 10 kV, MOSFETs are less efficient than IGBTs, or thyristors. In other words, with the increase of blocking voltage, bipolar devices are preferred. The on-state losses in bipolar structures are lower compared to unipolar ones due to conductivity modulation: the thick low doped blocking layer of the diode or switch is flooded by injection of carrier from highly doped electrodes. With full modulation these devices represent constant voltage drop independent of current. However, the modulation is not easy to achieve. For voltages in the 10-20 kV range, the thickness of the blocking layer varies between 100 and 200 microns. This implies that injected carriers need to diffuse comparable distances before recombining which, in turn, corresponds to carrier lifetimes in the 2-5 microsecond range. This figure together with extended defect densities could be used as the figure of merit for the Sic blocking layer quality.

Blocking layers for high voltage devices are presently grown by silane-based chemical vapor deposition (CVD) at temperatures between 1500 and 1650°C. This method allows for controlled and reproducible growth of n-type or p-type films with the concentrations of residual uncompensated donors or acceptors in the range of 10^{14} cm^{-3}. The typical lifetime values in high quality layers approach 1 µs. However, there are several problems that still have not been fully resolved. One of them is a relatively low growth rate in the 3-10 µm/hr range which makes the silane-CVD process exceedingly expensive. Another is the polytype instability: 2D nucleation during epitaxy at temperatures below 1800oC leads to formation of cubic polytype inclusions of different thicknesses. Since the required extended defect densities in high voltage devices are below 1 cm^{-2}, the polytype instability can result in significant yield loss.

The goal of this research project was to demonstrate novel approach to SiC growth that could alleviate problems listed above. Specifically, we set out to investigate the factors controlling carrier lifetimes in material grown at high deposition rates. The growth technique used was Halide Chemical Vapor Deposition. This technique is a modification of a standard CVD process using halogenated silicon precursor SiCl4 in conjunction with propane. Deposition is carried out at temperatures close to that of

3

PVT growth. That allows for growth of SiC crystals at high growth rates with low doping concentrations. The distinguishing features of this method are the separate injection of the silicon and carbon precursors into the reactor and the preheating of the reactants in the injectors which is made possible by much higher stability of the SiCl4 precursor compared to silane.

2. Experimental

The HCVD reactor has a vertical impinging jet configuration, with process gases fed upwards through graphite injectors while seed wafer is mounted horizontally facing down towards the injectors (Fig. 2.1). The exhaust gases are extracted at the bottom of the reaction zone which is surrounded by a cylindrical graphite susceptor. The hot zone is enclosed by graphite foam insulation in order to reduce the radiative heat loss. The entire assembly is located inside the water-cooled double-wall quartz tube. The mixture of propane and hydrogen is supplied via the inner injector while $SiCl_4$ in the Ar carrier gas is delivered via the outer injector. Flow rate of each gas was controlled by Mass Flow Controllers (MFC). The flows of all gas components are given as readings of corresponding MFCs with the exception of $SiCl_4$ due to its high vapor pressure. For calibration, weight change of the $SiCl_4$ bubbler was measured after each run so that the actual number of moles of $SiCl_4$ flown in the process was known and could be directly correlated with flow values measured by the MFC. The volume flows of SiCl4 quoted below were converted from moles using Boyle-Marriott law. Growth temperature was measured by a two-color pyrometer focused on the top of the crucible lid through the opening in the graphite insulation. The susceptor was inductively heated by a 50 kW generator operating at the frequency of approximately 10 kHz. The HCVD reaction zone is similar in shape and temperature distribution to that used for PVT growth.

After loading the graphite hot zone, the reactor was sealed and baked out. After overnight pumping with a turbomolecular pump, temperature was increased slowly over several hours in order to outgas the graphite parts. After the temperature reached 1050°C, the furnace was backfilled with argon to the pressure of 600 Torr and the temperature was increased slowly to the growth temperature. Growth experiments were performed in the temperature range between 1800°C and 2150°C at pressures between 40 and 400 Torr. Commercially available Si-face 6H- and 4H-SiC wafers were used as seeds.
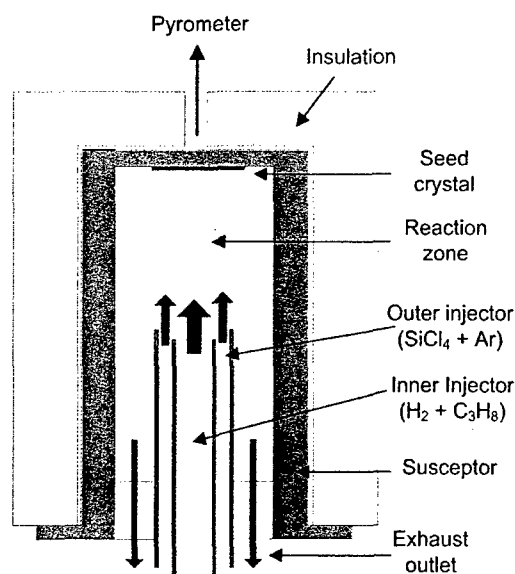
Figure 2.1 Schematic drawing of the Halide CVD hot zone showing orientation of the gas flow and the location of the seed crystal.

Electrical properties of HCVD material were measured on 1×1 cm2 pieces by removing the n^+-SiC substrates. The growth surface of the crystals (Si face) was lapped, polished, cleaned in acetone and methanol, etched in 10% HF, and rinsed in de-ionized water. Ohmic contacts were prepared at the corners of the sample by sputtering of either Ni for conducting samples or Au/Cr/Ta for high-resistivity samples. The contacts were annealed at 950°C for 15 min in forming gas. Capacitance-voltage (C-V) and deep-level transient spectroscopy (DLTS) measurements were performed on circular Ni diodes approximately 500 µm in diameter which were sputtered using a shadow mask. The carrier concentrations and mobilities at room temperature were obtained through standard van der Pauw and Hall-effect measurements with magnetic field of 0.4 T. Resistivities, carrier concentrations, and mobilities on highly resistive samples were measured from room temperature to 1000 K using a specially designed hot stage with very low leakage. Similar measurements in the temperature range from 77 to 800 K were performed for some of the samples by using a gas-flow cryostat.

A deuterium UV lamp was used as a means of optical injection in DLTS variant henceforth referred to as ODLTS. Capacitance transients were measured with an HP4280A C-t meter and an HP8112A pulse generator. At each temperature point the entire capacitance relaxation curve was captured and processed in the usual way with selected time windows. Typically 100 points were taken on each relaxation curve,

with the time between the points of usually 100 ms. Measurements were carried out for temperatures between 85 and 400 K. The length of the light pulse was between 2 and 5 s. Concentrations of nitrogen, boron, aluminum, vanadium, and titanium were measured by secondary-ion-mass spectrometry (SIMS). A raster scan technique was used in order to increase the sensitivity to nitrogen. Photoluminescence measurements were performed at 1.6 K using the 351 nm UV line of an Ar+ ion laser for excitation. The excitation power density was varied from 0.25 to 75 W/cm^2. The emission was analyzed by a 0.25 m double-grating spectrometer and detected by a GaAs photomultiplier tube. Electron paramagnetic resonance (EPR) measurements were performed at 20 K in a Bruker EMX X-band (9.5 GHz) spectrometer. Several series of growth experiments were performed. In series I, hydrogen flow was equal to or lower than 2 slm and the length of the inner injector carrying the H_2/C_3H_8 mixture was the same as the length of the outer injector carrying the $Ar/SiCl_4$ mixture. This resulted in longer residence time of H_2/C_3H_8 in the injector and conditions closer to equilibrium than for other growth series. Under these conditions, the effective C/Si ratio was determined by the value of the hydrogen flow rather than by the ratio of the propane and $SiCl_4$ flows. All other series of samples were grown with the inner injector shorter than the outer injector and a hydrogen flow of 3 slm. In this case, the composition of the gas phase near the growing SiC crystal was governed by the ratio of C_3H_8 and $SiCl_4$ flows. In series II, the C/Si flow ratio was varied by changing the flow of $SiCl_4$ and all substrates were on axis. Series III used substrates miscut 3.5° toward $[11\overline{2}0]$. In series IV, the substrates were 3.5° off axis and the C/Si ratio was varied by varying the C_3H_8 flow while keeping the $SiCl_4$ flow constant.

Table 3.1 Heat of formation for various Si-precursors used for SiC CVD.

Compound	ΔH_{fo} (kcal/mol)	Reference
SiH_4	8.2	1
$(CH_3)_3SiCl$	-86.3	2
$(CH_3)_2SiCl_2$	-113.7	2
$(CH_3)SiCl_3$	-137.8	2
$SiCl_4$	-158.4	2
Si_2Cl_6	-232.7	2

Kingon et al. [1] and Fishman and Petuskey [2] investigated the stability of various condensed phases in the Si-C-Cl-H system for a wide range of compositions of reactants in the temperature range of 700°C-

1700°C. They reported on the possibility of co-deposition/single phase deposition of Si, SiC and C, depending on the reactant flow, pressure, and temperature. However, their calculations were limited to temperatures below 1700°C and did not take into account the alternate mechanism of hydrocarbon transport to the reaction zone provided by hydrogen-etching of graphite parts at elevated temperatures, as suggested by Rottner and Helbig [3].

Thermodynamic modeling was performed using the HSC Chemistry code (Outokumpu Research Oy., Pori, Finland). The calculations were based on the minimization of free energy for a system defined by a fixed temperature, fixed total pressure, and fixed amounts of the input species [4]. The list of vapor species considered for the analyses include: CH, CH_2, CH_3Cl, CH_4, CH_3, C_3, C, C_2HCl, C_2H, C_2H_4, C_2H_2, C_3H_8, Cl, Cl_2, H, H_2, HCl, Si_3, Si, Si_2, SiC, SiC_2, Si_2C, $SiCl$, $SiCl_2$, $SiCl_3$, $SiCl_4$, SiH, SiH_3Cl, $SiHCl_3$, and SiH_2Cl_2. α-SiC, Si, and C (graphite) were considered as the only condensed phases present in the system. At the temperatures of interest, α-SiC is the stable polytype [5]. Unless otherwise stated, the Figures in this paper show the gas phase composition (solid phases are denoted by subscript-'s'). Calculations were performed in two steps. First, the reactant gas mixtures in the respective injectors were equilibrated with graphite. In the second step, a thermodynamic equilibrium between the dominant species as calculated from the first step was considered to model SiC growth. Such analysis could predict the trends in the growth rates to the first order only. The input amount of C (graphite) used in the first step of calculations was arbitrarily assigned a large value of 1000 mol to depict the ambient conditions inside the graphite injectors. The ratios of input amount of other reactant species in the calculations were the same as the ratio of their respective input volumetric flow rates.

Figure 3.1 shows the result of thermodynamic calculations under the conditions expected inside the outer injector with $SiCl_4$ and Ar gas mixture. The input amounts of Ar, $SiCl_4$ and C (graphite) used in the calculations were 1800 mol, 222 mol, and 1000 mol, respectively. The equilibrium gas phase composition is plotted as a function of temperature. $SiCl_4$ remains largely undissociated for temperatures lower than 1700°C (not shown in the figure). At higher temperatures it dissociates primarily into $SiCl_x$ (x=1,2,3) and Cl. The concentration of $SiCl_3$ reaches maximum at about 1950°C and decreases with further increase of temperature. Concentrations of $SiCl_2$, Cl, SiCl, and Si increase with temperature and then saturate above 2200°C. The amount of C_2Cl_2 which is the most dominant of the C-bearing species, is four orders of magnitude lower than the primary Si-bearing species, $SiCl_2$, suggesting that the etching of the graphite injector should be negligible. There are no condensed phases formed for the investigated temperature range and concentrations of $SiCl_4$. This implies that there will be no deposit formed in the

7

injector. This is different than the silane-based process as it decomposes readily at temperatures above 700°C. The formation of solid Si and SiC can lead to blocking of reactor inlets and restricts the range of flows for High Temperature SiC CVD process [6].
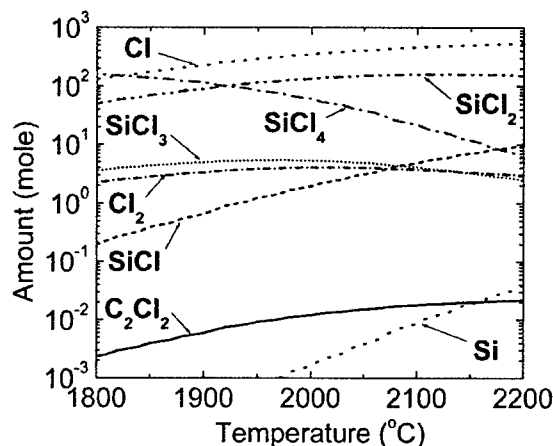

Figure 3.1 Calculated equilibrium amounts of dominant species in the $SiCl_4$+Ar injector as a function of temperature at 200 Torr. The input amounts of Ar, $SiCl_4$ and C (graphite) used in the calculations were fixed at 1800 mol, 222 mol and 1000 mol.

The results of heating a dilute C_3H_8 gas mixture in the H_2 carrier gas inside the inner injector are:

(i)   the decomposition of the C_3H_8 into more stable gaseous components, mainly C_2H_2 [7],

(ii)   deposition of solid graphite as a product of C_3H_8 decomposition [3], and

(iii)   etching of graphite by H_2 with the formation of various gaseous hydrocarbons, predominantly C_2H_2 [3].

Figure 3.2 shows the result of thermodynamic calculations, depicting the compositions of dominant species for the mixture of C_3H_8, H_2, and graphite as a function of temperature. The species with amount less than 10-3 mole are not shown to avoid congestion. The input amounts of C_3H_8, H_2, and graphite were held constant at 8.5 mol, 3000 mol, and 1000 mol, respectively. The amounts of all the hydrocarbon species increase with temperature except CH_4 and C_2H_4. These results show a similar trend in composition of different hydrocarbon species as reported by Rottner and Helbig [3]. Their calculations also predict a decreasing concentration of CH_4 and show C_2H_2 as the most dominant C-bearing specie at temperatures above 1625°C. Presence of significant amount of C_2H at high temperature is also consistent

8

with their reports and is contrary to the models which were proposed earlier [2,7] where hydrogen etching of the graphite parts was not considered. It was also reported, that for temperatures above a certain critical temperature (T_C), 70-80% of the equilibrium concentration of hydrocarbons is supplied through the hydrogen etching of the graphite parts and the remainder is supplied via the input C-precursor such as propane. The situation is reversed below T_C. T_C is dependent on the effective graphite surface area, flow rate of the input C-precursor, and partial pressure of hydrogen [8]. It can be expressed as:

$$T_C = -\frac{H_D}{R}\left[\ln\left(\frac{mQ}{60V_m AK_{SR}p_{H_2}p_o}\right)\right]^{-1} \qquad (1)$$

where R is the universal gas constant, R = 8.314 J/mol. K; m is the number of moles of carbon per mole of input gas, m = 3 for C_3H_8; Q is the flow rate of C-precursor (equal 4.5-17 sccm in our case); V_m is the molar volume = 22300 cm^3/mol; A is the active graphite area for the inner injector (equal 37.2 cm^2 assuming that the active and geometric areas are close to each other due the presence of dense pyrolytic graphite deposit inside the inner injector); p_{H_2} is the partial pressure of hydrogen (p_{H_2} ~ 0.263 atm in all our experiments); and H_D, K_{SR}, and p_o are constants given as [8]: K_{SR} = 120 $\mu mol.s^{-1}.cm^{-2}.atm^{-3/2}$, p_o = 1410 $atm^{1/2}$, and H_D = 226 kJ/mol. The calculated value of T_C for our reactor under the reaction kinetics controlled regime (explained later in this paragraph) was approximately 2000°C. Based on the discussion of Rottner and Helbig, there are two different regimes possible, one in which the hydrocarbon supply inside the inner injector is determined by the etching of the graphite by hydrogen and increases linearly with input hydrogen supply (referred to as "thermodynamic equilibrium limited regime" in the later part of this report), and second, in which the hydrocarbon supply is determined by the flow rate of C-precursor ("reaction kinetics controlled regime"). The latter allows for independent control of Si- and C-bearing species and it is typically preferred in most CVD systems. This requires T_C to be as large as possible. Large T_C could be achieved by either decreasing the effective graphite area and/or by increasing the linear propane flow velocity.
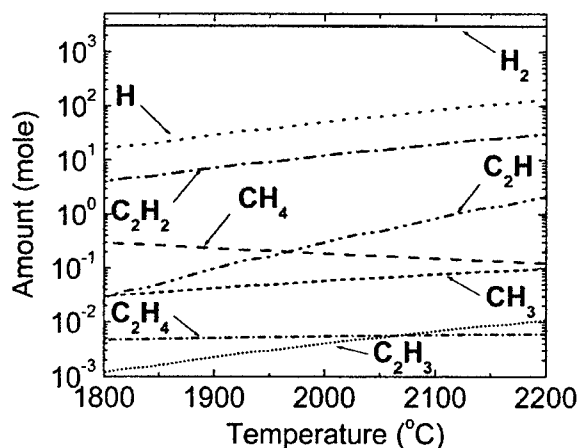
Figure 3.2 Calculated equilibrium amount of dominant species in the $C_3H_8+H_2$ injector as a function of temperature at 200 Torr. The input amounts of H_2, C_3H_8 and C (graphite) used in the calculations were fixed at 3000 mol, 8.5 mol and 1000 mol.

The chemical reactions that occur in the reaction zone are rather complex. Figure 3.3 shows the calculated equilibrium concentrations of the dominant species at the temperature of 2050°C and the pressure of 200 Torr as a function of the number of moles of the $SiCl_4$ at the input, with other input species of hydrogen, propane and graphite fixed at 3000 mol, 8.5 mol and 100000 mol, respectively. These input values are the same as the values of gas flow rates from one of experimental conditions. In calculations, propane did not make any significant contribution to results. $SiCl_4$ dissociates into $SiCl_2$ and Cl, followed by the reaction with hydrogen and formation of gaseous HCl. The dominant gaseous silicon bearing species are the $SiCl_2$ radicals while the dominant carbon bearing species are the C_2H_2 molecules. For the low amount of $SiCl_4$, the formation of SiC increases with linearly with $SiCl_4$. With amount of $SiCl_4$ exceeding 200 mole, the SiC formation curve shows a broad maximum followed by decrease to almost zero. This is due to the decrease of the hydrogen and hydrocarbons concentrations available for the reaction and the increased amount of gaseous HCl in the vapor which will prevent further dissociation of $SiCl_2$. The reaction between $SiCl_2$ and hydrogen to form HCl and SiC, will not proceed because one of the reaction products, HCl is already dominant and exceeding the concentration of one of the reactants, hydrogen. Therefore, with the further increase of $SiCl_4$ over 200 mole, hydrogen decreases, HCl and $SiCl_2$ increases and, eventually, SiC formation decreases. With more than 1200 mole of $SiCl_4$, most of the $SiCl_2$ molecules remain unreacted and little solid SiC will form.
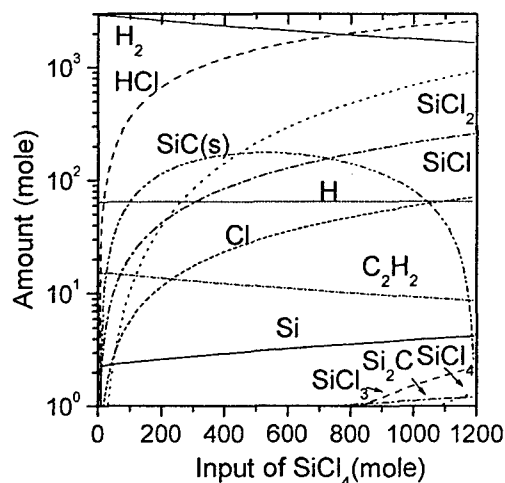
10

Figure 3.3 Calculated equilibrium concentration of dominant species as a function of SiCl4 content at 2050°C and 200 Torr. Amount of H2, C3H8 and carbon are fixed at 3000 mol, 8.5 mol, and 100000 mol, respectively.

Figure 3.4 shows the comparison between the calculated equilibrium amounts of SiC formed in the reaction zone (dashed curve and left axis) and the experimental data (filled squares (■) and right axis) at 2050°C, as a function of SiCl4 amount at the input. The amounts of C_3H_8, H_2 and C (graphite) at the input were fixed at 8.5 mol, 3000 mol, and 1000 mol, respectively, for the thermodynamic calculations, whereas, the input flow rates of C_3H_8 and H_2 were maintained constant at 8.5 sccm and 3000 sccm during the growth experiments. The amount of SiC formed increases rapidly for low flow rates of $SiCl_4$ and then saturates for higher flows when the supplies of hydrogen and carbon are exhausted. These results suggest that in the low flow regime, stoichiometry of the gas phase can be controlled by varying the $SiCl_4$ flow rate.

Figure 3.5 shows the results of calculations for the amount of SiC formed in the reaction zone as a function of hydrogen flow at three different values of $SiCl_4$. The top curve (dotted line) corresponds to an input $SiCl_4$ amount of 148 mol, middle curve (dashed line) to 74 mol and the bottom curve (solid line) to 37 mol. The concentrations of all hydrocarbons were calculated assuming equilibrium in the $C_3H_8+H_2$ injector (Figure 3.2) corresponding to the given input hydrogen flow. In such series of experiments, the SiC amount increases approximately linearly for low input amount of hydrogen (less than 1000 mol) suggesting Si-rich conditions in the reaction zone. The equilibrium amount of SiC saturates for high input amounts of hydrogen and the SiCl4 amount of 37 mol. This corresponds to the composition of the gas

11

mixture becoming C-rich. At higher input SiCl4 amounts, the composition of the gas mixture remains Si-rich and the amount of SiC increases approximately linearly with the supply of hydrocarbons to the reaction zone. It should also be noted that for low hydrogen input amount (less than 1000 mol), the calculations predict a decrease in the amount of SiC with an increase in input $SiCl_4$ amount. This is most likely due to the depletion of hydrogen and hydrocarbons available for the reaction and to the etching of SiC by HCl present in the gas phase.
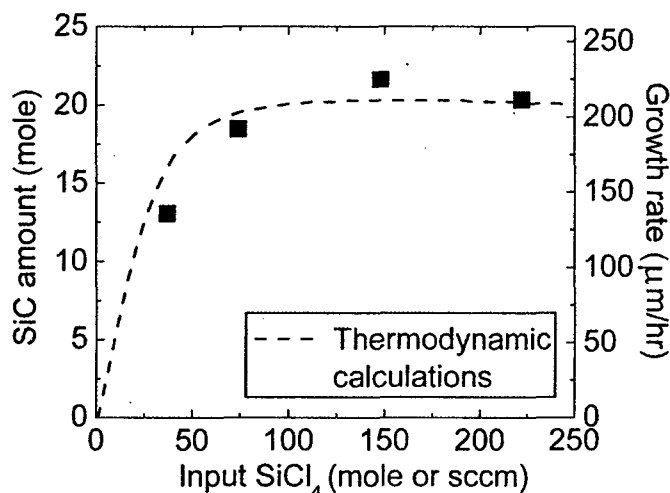

Figure 3.4 Comparison between the calculated equilibrium amounts of SiC (dashed line) formed in the reaction zone at 2050°C and 200 Torr and the experimental growth rates (■) as a function of $SiCl_4$ flow. The amount of H_2 was fixed at 2000 mol. The amounts of C-bearing species were calculated assuming the thermodynamic equilibrium between the H_2-propane gas mixture and graphite (Figure 3.2).

The results of calculation for the outer injector show that $SiCl_4$ thermally decomposes at temperatures above 1700°C producing $SiCl_x$ (x=1,2,3) vapor species. In parallel, propane decomposes to simpler hydrocarbons, primarily C_2H_2 and C_2H. Hydrogen plays a dual role, acting as the carrier gas for hydrocarbons and also reducing $SiCl_x$ species in the reaction zone. The subsequent reactions between the Si- and C-bearing species lead to the formation of SiC.
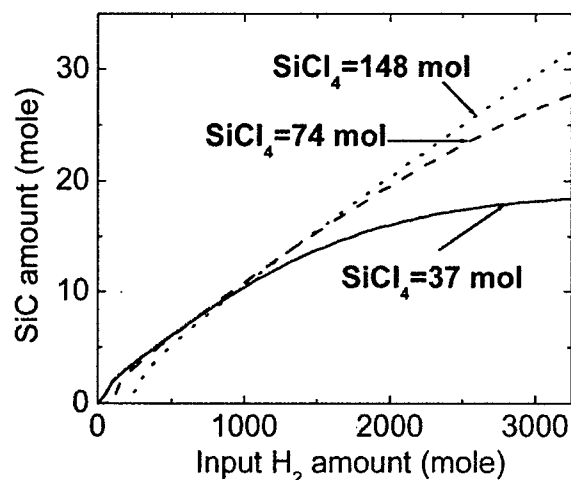
Figure 3.5 Calculated equilibrium amounts of SiC formed in the reaction zone at 2050°C and 200 Torr as a function of H_2 amount for three different quantities of $SiCl_4$. The amounts of C-bearing species were calculated assuming the thermodynamic equilibrium between the H_2 flow and graphite (Figure 3.2).

4 Growth rate experiments

The growth rates mentioned in this paper are reported as the average of thicknesses measured over several locations on the quarter of two inch wafers that were used as seeds, divided by the growth time. Based on accumulated statistics of over two hundred growth runs, the growth rate error does not exceed 15%.

4.1 Thermodynamic equilibrium limited regime

Figure 4.1 shows the dependence of the SiC growth rate on C_3H_8 flows at constant hydrogen and $SiCl_4$ flow rates of 2000 sccm and 148 sccm at 2050°C. The propane flow rates were varied between 4.5 sccm and 17 sccm. The dependence of the growth rate on the propane flow in this range was very weak with the maximum change of the growth rate being less than the experimental error (15%). This dependence is the same as discussed earlier by Rottner and Helbig [3] where in the thermodynamic equilibrium limited regime, propane primarily compensates for the etching of the graphite parts by H_2.
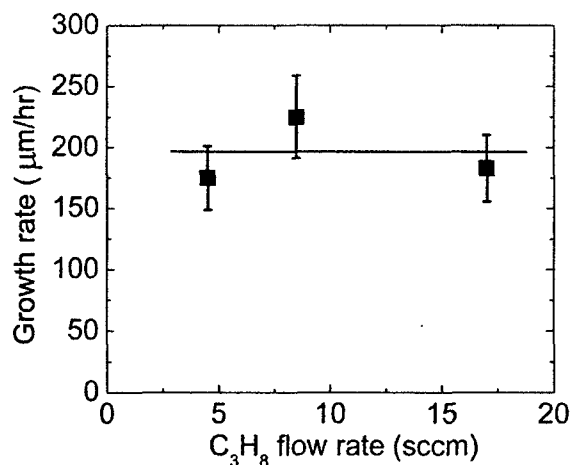
Figure 4.1 SiC growth rate as a function of C_3H_8 flow in the thermodynamic-equilibrium-limited-regime. The flows of $SiCl_4$ and H_2 were held constant at 148 sccm and 2000 sccm. Samples were grown at the growth temperature of 2050°C and a pressure of 200 Torr.

Figure 4.2 shows the experimental data on SiC growth rate as a function of H_2 flow at three different flows of $SiCl_4$ in the thermodynamic equilibrium limited regime. The lower curve (line with filled triangles (▲)) corresponds to $SiCl_4$ flow rate of 37 sccm, the middle curve (line with filled circles (●)) to $SiCl_4$ flow rate of 74 sccm, and the upper curve (line with filled squares (■)) to $SiCl_4$ flow rate of 148 sccm. The hydrogen flow rate was varied between 500 to 3000 sccm whereas the C_3H_8 flow rate was held constant at 8.5 sccm. The growth temperature was held constant at 2050°C. The trend in the growth rate variation with the hydrogen flow is very similar to that predicted by the thermodynamic calculations (Figure 3.5) for the hydrogen flow rates up to 2000 sccm. At higher hydrogen flow rates, the experimental growth rates decrease rather than saturate. This effect can be understood by analyzing the role of hydrogen in the HCVD reactor – (i) to reduce $SiCl_x$ species, (ii) to transport hydrocarbons due to the etching of graphite parts, (iii) to supply C-precursor to the reaction zone, and (iv) to etch the SiC crystal. If we assume that the C-transport to the reaction zone by (ii) and (iii) compensates each other with the increase in the linear flow velocity of hydrogen, then the decrease in the SiC growth rate with hydrogen flow can be explained on the basis of (i) and (iv). With the decrease in $SiCl_4$ flow rates, the unreacted hydrogen responsible for SiC etching increases with the hydrogen flow. The byproducts of etching reactions are continuously flushed out of the reaction zone, thus preventing equilibrium to establish near the surface of the grown crystal. This continuous etching with removal of exhaust gases leads to the decrease in the SiC growth rate with increase in hydrogen flow. On the other hand, thermodynamic calculations assume complete equilibrium being established between the reactant gases

14

and the SiC substrate (batch process) thus, predicting saturation in growth rate with increased hydrogen flow. These results further suggest that the stoichiometry of the gas mixture in the reaction zone can be varied by controlling the input flow rate of hydrogen into the reactor. The growth rate dependence on the $SiCl_4$ flow rate under the thermodynamic equilibrium limited regime has been presented earlier in discussion of Figure 3.4.
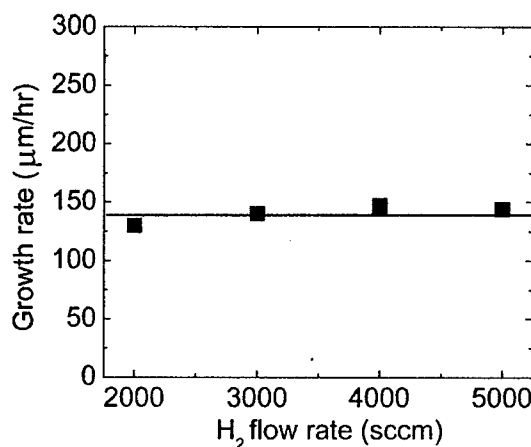

Figure 4.2 Experimental SiC growth rate as a function of the H_2 flow at three different flows of $SiCl_4$ for the thermodynamic equilibrium limited regime. Samples were grown at the growth temperature of 2050°C, pressure of 200 Torr and C_3H_8 flow at 8.5 sccm. The lines serve only as guide to the eye.

The downsides of operating in the thermodynamic-equilibrium-limited regime are related to stronger hydrogen etching of the grown crystal with increased hydrogen flow and difficulty in achieving efficient mixing of the Si-bearing and the C-bearing gas fluxes in the reaction zone for high hydrogen flows (>2000 sccm). The first effect limits the range of the gas phase compositions achievable with HCVD and the second affects the uniformity of SiC deposition over large diameter seeds.

4.2 Reaction kinetics controlled regime

The thermodynamic-equilibrium-limited regime is not always predominant in HCVD growth. By changing the reactor configuration so as to decrease the temperature at the top of the inner injector (making it lower than T_C), and shortening the residence time of the gas mixture, we have observed a significantly different behavior. This was achieved by shortening the length of the inner injector and reduction of the injector cross section area. In order to verify the kinetic-limited regime, we held the

SiCl$_4$ and C$_3$H$_8$ flow rates constant at 148 sccm and 8.5 sccm and varied hydrogen flow rates between 2000 sccm and 5000 sccm, at 2050°C. The growth rate was constant at about 140 µm/hour and independent of the hydrogen flow rate. This is distinctly different behavior compared to linear dependence observed under the Si-rich conditions for the thermodynamic limited regime discussed earlier.

Figure 4.3 shows the growth rate versus propane flow. The H$_2$ and SiCl$_4$ flows were maintained constant at 3000 sccm and 222 sccm, respectively. The growth rate increases linearly with propane flow and indicates that the growth was carbon-limited. This also indicates Si-rich growth ambient. Under such regime, the supply of C-bearing species to the reaction zone strongly depends on the propane flow rate and is no longer controlled by the local thermodynamic equilibrium established between the graphite assembly and the reactant gases. This can be concluded by comparing above results with Figure 6 where the growth rate dependence on propane flow rate was very weak. Extrapolation of growth rate to zero flow rate of C$_3$H$_8$ should result in growth rates of approximately 75 µm/hr. This in turn, should correspond to the hydrocarbons from the etching of graphite by hydrogen which is a significant contribution to the total hydrocarbon supply to the reaction zone for low flow rates of C$_3$H$_8$ (< 10 sccm). At higher C$_3$H$_8$ flow rates, the majority of hydrocarbons (70-80 %) supplied to the reaction zone should correspond to thermal decomposition of C$_3$H$_8$ which is characteristic of reaction kinetics controlled regime.
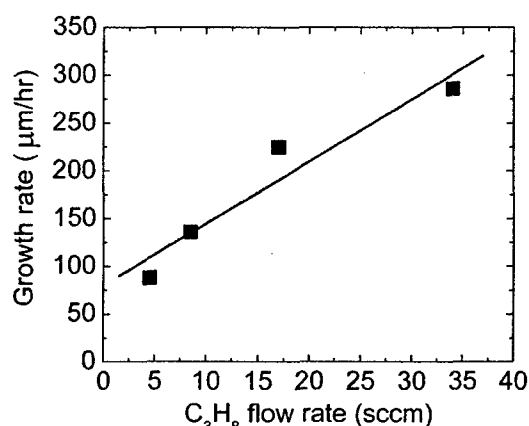

Figure 4.3 SiC growth rate as a function of C$_3$H$_8$ flow in the reaction kinetics controlled regime. The SiCl$_4$ and H$_2$ flow rates were held constant at 222 sccm and 3000 sccm, respectively. Samples were grown at the growth temperature of 2050°C and a pressure of 200 Torr.

In order to determine the dependence of the SiC growth rate on input flow rates of $SiCl_4$, the H_2 and the propane flows were fixed at 3000 sccm and 8.5 sccm, respectively and $SiCl_4$ flow rates varied between 37 sccm to 300 sccm. The growth temperature was held constant at 2050°C. The results are presented in Figure 4.4. The growth rate increased linearly at low $SiCl_4$ flows and saturated at high $SiCl_4$ flows. This behavior can be interpreted as due to silicon-supply-limited growth at low $SiCl_4$ flow rates becoming carbon-supply-limited at high $SiCl_4$ flow. The observed trend is similar to the one presented for thermodynamic equilibrium limited regime earlier. This is expected as the only difference between the two regimes is the supply of hydrocarbons to the reaction zone which was constant in this series of experiments. One does not expect any difference in the supply of Si-bearing species to the reaction zone for the two regimes except for the second order effects associated with reduced length of the inner injector and change in the flow pattern. The latter effect is evident by comparing the growth rates for the thermodynamic equilibrium limited regime and reaction kinetics controlled regime for the same $SiCl_4$ flow. The growth rates for the latter are approximately 30 percent lower than the former (in the saturation region of the growth rates), which could be attributed to decrease in mass transport due to increased separation between the seed crystal and the inner injector in the reaction kinetics controlled regime.
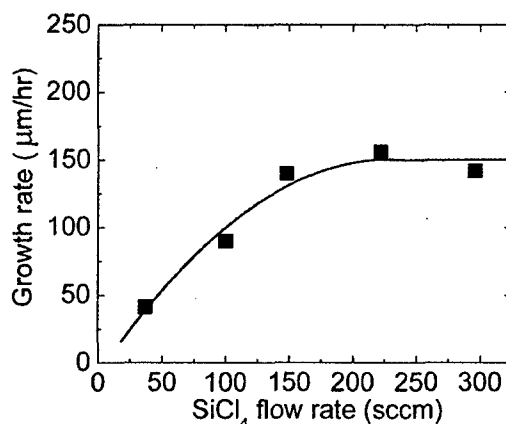

Figure 4.4 SiC growth rate as a function of $SiCl_4$ flow at a fixed C_3H_8 flow of 8.5 sccm and a fixed H_2 flow of 3000 sccm under the reaction kinetics controlled regime. Growth temperature was 2050°C and the pressure 200 Torr.

The results presented in this section are characteristic of a reaction-kinetics-controlled growth where the gas phase composition is determined by the ratio of flows of $SiCl_4$ and C_3H_8. These results also suggest that the temperature closer to the top of the inner injector was less than T_C. This, however, could change with the change of growth temperature.

4.3 Temperature dependence of growth rate

Since the reaction rates are expected to increase with the growth temperatures, the shortening of the inner injector might not be enough to assure the reaction-kinetics-controlled regime at high growth temperatures. Here we simply present the changes in the growth rate as a function of temperature without detailed study on the flow rate dependence at respective temperatures. The results are presented in Figure 4.5. The dashed curve shows the results of thermodynamic calculations (left axis), whereas, the filled squares (■) correspond to the experimental data (right axis). For the thermodynamic calculations, the amounts of $SiCl_4$, H_2, and C_3H_8 were held constant at 74 mol, 1000 mol, and 4.5 mol, with graphite held at 1000 mol. During the experiments, the flow rates of $SiCl_4$, H_2, and C_3H_8 were held constant at 74 sccm, 4.5 sccm, and 1000 sccm. Experiments were limited to the temperature range between 2000°C to 2150°C since, for temperatures lower than 2000°C, a parasitic deposit of polycrystalline SiC was observed over the top of the inner injector. This deposit resulted in partial blocking of the inner injector preventing the stable growth. Using the injector with shorter length (as used in the reaction kinetics controlled regime) and higher flow rates of reactant gases (greater than 1000 sccm H_2, 74 sccm $SiCl_4$, and 4.5 sccm C_3H_8), at growth temperatures below 2000oC, resulted in increased rate of parasitic deposit over the top of the inner injector. Growth experiments for temperatures greater than 2150°C were not carried out due to technical issues.
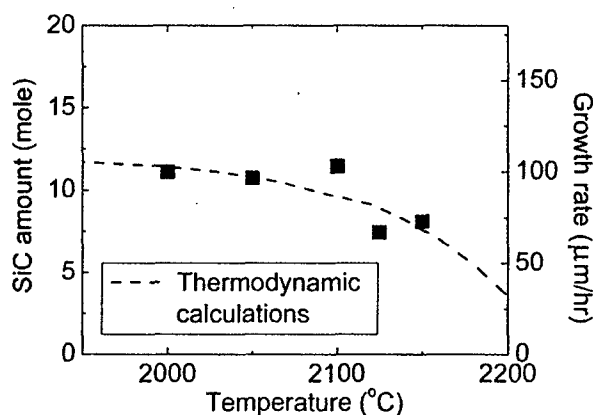

Figure 4.5 SiC growth rate as a function of growth temperature. The dashed curve shows the result of thermodynamic calculations (left axis). The $SiCl_4$, C_3H_8, H_2 and C (graphite) amounts 74 mol, 4.5 mol, 1000 mol, and 1000 mol, respectively. The filled squares (■) represent the experimental growth rates (right scale). The flow rates of $SiCl_4$, C_3H_8, and H_2 were maintained constant at 74 sccm, 4.5 sccm and

1000 sccm respectively. The pressure was held constant at 200 Torr during both calculations and experiments.

The thermodynamic calculations show a decrease of approximately 40% in the growth rate for the investigated temperature range (2000°C – 2150°C) which agree with experimental data. The decrease in the growth rate is most likely related to enhanced evaporation and etching of the surface of the crystal. In order to explore a wider temperature range for growth than discussed above, it is essential to optimize the flow rates of reactant gases and make appropriate changes in the reactor configuration such that high growth rates can be sustained and formation of parasitic deposits at lower temperatures can be avoided. Such optimization studies are being presently carried out.

5 Properties

As stated in the Section 1. Goals, the two figures of merit for the quality of SiC materials for the high voltage applications are extended defect density and carrier lifetimes. This project was primarily concerned with the control and understanding of carrier lifetimes.

5.1 Residual impurities and electrical properties

SIMS measurements performed on representative samples grown in all four series of experiments described above showed that the concentrations of typical shallow acceptors, aluminum, and typical deep level impurities, vanadium and titanium, were below the detection limits (5×10^{13} cm^{-3} for Al, 5×10^{12} cm^{-3} for Ti, and 3×10^{11} cm^{-3} for V). The only important impurities detected by SIMS were nitrogen and boron. For nitrogen, a decrease of concentration by a factor of several was observed with increase of the C/Si ratio from 0.065 to 0.7, as illustrated in Fig. 5.1. The data in the figure refers to miscut samples grown in series III and series IV growth experiments. The nitrogen density changes shown in the figure are consistent with the site competition effect.[9, 10] Boron concentration showed a clear tendency to increase with increasing the C/Si ratio, as illustrated in Fig. 2. The trend again is similar to the one observed in CVD epitaxy and is explained by B preferring to occupy Si sites in growth ambient involving hydrogen.[10, 11] In that case, increasing the C/Si ratio favors incorporation of boron due to the site competition effect.
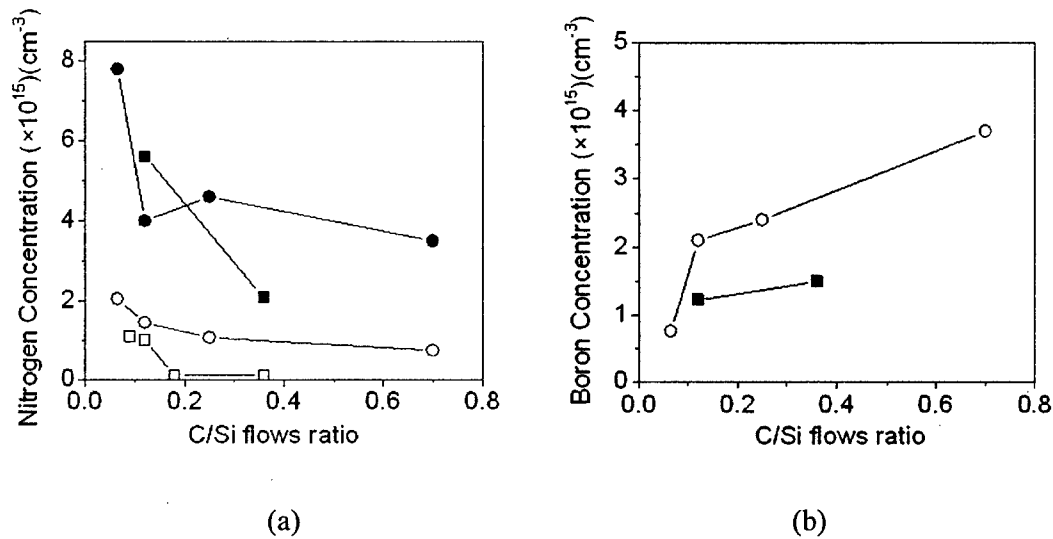
Figure 5.1 Nitrogen (a) and boron (b) concentration dependence on the C/Si flow ratio in two series of growth runs (squares - series III, circles - series IV); solid lines correspond to SIMS measurements, dashed lines to LTPL measurements.

One of the systematic trends observed in al samples, was that the nitrogen concentration was considerably lower in on-axis samples compared to off-axis samples grown in otherwise similar conditions. This effect is illustrated in Table 5.1 for two pairs of samples differing from each other only by the miscut angle. Changes observed in the boron concentration measured in off-axis and on-axis samples were not so pronounced (Table 1.2). A detailed explanation is lacking at the moment, but it has been reported that in samples prepared by CVD epitaxy, nitrogen concentration increased significantly with increasing the miscut angle while aluminum concentration did not change much as a function of miscut [12] [13] [14]. By way of explanation, it was suggested that nitrogen attaches itself to steps on the surface of SiC. Since the density of steps increases with increased miscut angle this should account for the corresponding increase in nitrogen concentration. For aluminum, it was proposed that it attaches to the growth terraces which explains a weak dependence of Al concentration on miscut angle [14]. It is possible that similar phenomena are responsible for the difference in nitrogen and boron behavior observed in HCVD-grown on-axis and off-axis samples if boron acts similarly to aluminum. This is plausible because they also occupy Si sites.

Table 5.1 Concentrations of nitrogen and boron in two 6H-SiC crystals grown by HCVD, one on an on-axis seed and the other on an off-axis seed.

Sample #	Growth conditions	[N], cm-3 SIMS	[B], cm-3 SIMS	[N], cm-3 PL
H101, series II	On-axis, C/Si=0.12	3×10^{14}	1.2×10^{15}	1×10^{14}
H105, series III	Off-axis, C/Si=0.12	5.6×10^{15}	1.2×10^{15}	1×10^{15}
H86, series I	On-axis, C/Si=0.12	1×10^{15}	3.8×10^{15}	3.3×10^{14}
H97, series I	Off-axis, C/Si=0.12	4.7×10^{15}	8.2×10^{14}	2.8×10^{15}

Nitrogen donor concentrations were also estimated from the ratio of the intensity of the nitrogen-related bound exciton lines (R_o, S_o) to that of the free-exciton related phonon replica (I_{77}) in low temperature photoluminescence (LTPL) spectra of 6H-SiC [15] [16]. Corresponding calibration coefficients published by Ivanov et al. [16] are based on plotting these ratios versus the concentration of uncompensated shallow N donors obtained by capacitance-voltage C-V measurements. However, because the samples used were shown to be very lightly compensated, the conversion coefficients should give the entire concentration of the nitrogen donors provided they could be totally recharged by excitation light in LTPL experiments. This is a legitimate concern in cases for which the Fermi level is pinned below the nitrogen donors as found for a few samples in this work. The matter has been studied in detail recently for semi-insulating PVT-grown 4H-SiC where the Fermi level was pinned close to midgap such that all shallow N donors were compensated in the dark [17]. It was shown that the total concentration of nitrogen donors could be derived from the LTPL intensity ratios as long as one employed an excitation power condition where all the shallow donors were photo-neutralized (as evident by a saturation behavior in the PL ratio with increasing excitation light intensity). In particular, the dependence of the ratio of the bound-exciton to free-exciton lines was shown to be linear on the nitrogen concentration as determined by SIMS for residual [N] < 10^{16} cm^{-3} at excitation power densities of ~ 100 W/cm^2. The conversion coefficient obtained in these experiments was close to the one reported by Ivanov et al. based on C-V results for n-type SiC samples.

Photoluminescence spectra measured at 1.6K for two representative series of samples are shown in Figs. 5.2 (a) and (b). The PL lines in question are marked in the figures and it can be seen that in three of the four samples shown in Fig. a the ratio of the (R_o, S_o) to I_{77} intensities is quite low (~ 0.1). The power

density of the excitation light was changed for several of these samples from 0.25 to 75W/cm^2 to insure that saturation of the $(R_o+S_o)/I_{77}$ PL ratio was achieved. This is shown explicitly for one of the samples (H101) with C/Si ratio of 0.12 in Fig. (b). These ratios were converted to nitrogen concentrations using the conversion coefficient proposed by Ivanov et al. The dependence of the nitrogen concentration derived from LTPL measurements on the C/Si ratio for the two series of off-axis growth experiments is presented in Fig. 1 alongside the SIMS data. Most notably, the results show that the concentration of nitrogen in HCVD samples can be made as low as $\sim 10^{14}$ cm^{-3}.

It has, however, to be noted that the data in Fig. 5.1(a) show that the nitrogen concentration calculated from LTPL spectra are systematically lower than the SIMS results. This either means that the calibration coefficient proposed by Ivanov et al. should be increased (in our case, by about 3-4 times to fit the nitrogen concentration values measured by SIMS) or that there exist other centers involving nitrogen in 6H-SiC.
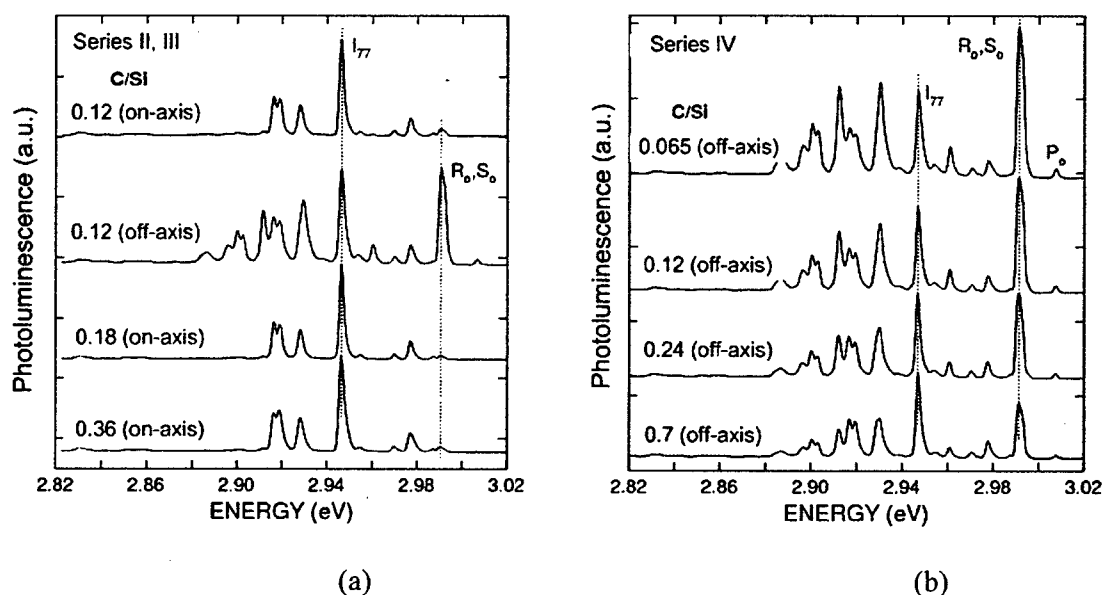

(a)   (b)

Figure 5.2 (a) LTPL spectra measured in the near-band edge region for several samples grown by HCVD with varying C/Si flows ratios for samples from (a) series II and (b) series IV; also shown in (a) is the spectrum measured for one of the series III samples grown off-axis with the C/Si ratio equal to 0.12 (sample H105). The spectra were obtained with excitation power density of 75 W/cm^2.

Electrical measurements shed additional light on possible nature of discrepancy between nitrogen concentrations measured by SIMS and LTPL and generally on the type of centers observed in SiC crystals

grown by HCVD. These studies were performed on the off-axis samples grown in the series IV samples. Hall effect and van der Pauw measurements at room temperature showed that samples H127, H125, H126 grown with C/Si ratios of 0.065, 0.12, 0.25, respectively, were n-type with electron concentration gradually decreasing from high 10^{15} cm^{-3} to high 10^{14} cm^{-3} as the C/Si ratio increased. Sample H128 grown with the highest C/Si ratio was semi-insulating (resistivity of 10^{10} Ωcm at room temperature) and showed p-type conductivity at high temperatures.

Fig. 5.3 presents the temperature dependence of electron concentration in the three n-type samples of this series. In sample H127 (C/Si=0.065) the temperature dependence at low temperatures had an activation energy of 0.14 eV and was close to the ionization energy of cubic-site nitrogen donors in 6H-SiC. It showed an additional step at high temperatures indicating the presence of deeper centers other than nitrogen donors. The two other n-type samples (H125 and H126) grown with higher C/Si ratio showed activation energy of 0.27 eV in the temperature dependence of electron concentration. Hence, nitrogen donors were totally compensated in these two samples and the Fermi level position was determined by deeper centers.
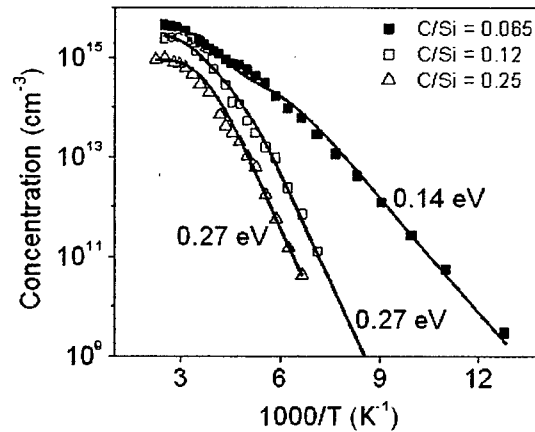

Figure 5.3 Temperature dependence of electron concentration in HCVD grown samples prepared on off-axis substrates with C/Si flow ratio of 0.065 (filled squares), 0.12 (open squares) and 0.25 (open triangles); the solid lines are fits using the electrical neutrality equation.

Experimental temperature dependences in Fig. 5.3 were fitted by solving the electrical neutrality equation taking into account cubic-site nitrogen donors N_{d1}, deeper centers N_{d2} assumed to be donors, and compensating acceptors N_a. N_a in these calculations presents the portion of the total acceptor

concentration that goes for the compensation of donors that pin the Fermi level at low temperatures (N_{d1} in sample H127 or N_{d2} in samples H125, H126). The full concentration of acceptors, N_A, exceeds N_a by the number of donors shallower than either N_{d1} or N_{d2} (depending on the Fermi level position): these shallower donors are completely ionized at all temperatures and their concentration cancels out the corresponding portion of acceptors in the neutrality equation. It is known, for example, that hexagonal-site nitrogen donors with ionization energy of 80 meV constitute half of the concentration of cubic-site donors N_{d1} at 140 meV and these two species are usually the main contributors to the shallow donor population. These 80 meV donors are totally compensated in sample H127 where the Fermi level is pinned by the cubic-site nitrogen donors. Correspondingly, the total number of compensating acceptors N_A should be close to $N_a+N_{d1/2}$. Naturally, in samples H125, H126 where the Fermi level is close to N_{d2} donors, N_A is higher than N_a by the concentration of all nitrogen donors, both cubic-site and hexagonal-site (to be precise, there are two types of cubic-site donors, equally populated, but these donors are generally indistinguishable in Hall measurements).

In electrical neutrality fitting calculations the degeneracy factor was assumed to be 2 for all donors, the number of equivalent minima in the conduction band was equal to 6 and the density of states effective mass was taken as $0.27m_o$ (m_o is the mass of free electrons). The results of fitting are shown as dashed lines in Fig. 5.3 and corresponding values of N_{d1}, N_{d2}, and N_a derived from the fitting are presented in Table 5.2. The ionization energies of N_{d1} and N_{d2} centers providing the best fit were respectively 0.14 eV and 0.27 eV. Centers with similar ionization energies have been reported for irradiated 6H-SiC samples [18] but not in as grown samples of epilayers grown by CVD or bulk PVT or H2PVT crystals. This leads us to conclusion that the activation energy of 0.27 eV is most likely associated with the 0.4 eV center seen in DLTS spectrum. This center was investigated in detail by Hemmingsson et al in 6H-SiC [19] as well as in 4H-SiC [20]. The center has two levels: an acceptor level located at 0.4 eV below conduction band and donor level at 0.2 eV. The donor level is not visible in standard DLTS. The capture cross-section of the acceptor level is thermally activated with the activation energy of 0.05 eV. When a negative-U center with such properties pins the Fermi level, the apparent activation energy is:

$$E_{HALL} = \frac{E_D + E_A}{2} = \frac{0.2 + 0.35}{2} \ [eV] = 0.275 \ [eV]$$

This energy is in perfect agreement with the results of Hall data.

In the most C-rich sample H128 of series IV crystals the concentrations of nitrogen and boron measured by SIMS were very close to each other. In agreement with that the sample was highly-resistive. At elevated temperatures the conductivity of the sample was p-type, with the activation energy of 0.6 eV (Fig. 5.4) close to the ionization energy of boron-related D-centers.[21],[22]
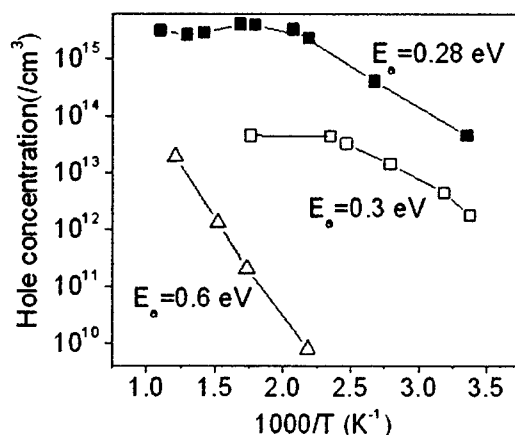
Figure 5.4 Temperature dependence of the hole concentration in three p-type HCVD samples: one grown on an on-axis substrate with C/Si flow ratio of 0.18 (sample H86, filled squares); second sample grown on an off-axis substrate with C/Si flow ratio of 0.36 (sample H102, open squares); and the third sample grown on an off-axis substrate with C/Si flow ratio of 0.7 (sample H128, open triangles).

The general behavior of resistivity with changing C/Si ratio was similar for all growth series and followed the trend described above for the series IV samples. At low C/Si ratio the samples showed n-type conductivity, the resistivity increased for intermediate C/Si ratios and at high C/Si ratios the samples became more or less highly resistive p-type. We note that the electron concentrations in n-type samples, the actual point where the n-p conversion occurred and the resistivity of p-type samples depended on the level of nitrogen and boron contamination. For example, in series III crystals, nitrogen and boron concentrations were considerably lower than in series IV crystals. Consequently, room temperature electron concentrations were lower in Si-rich samples and the transition from n-type to p-type occurred near C/Si=0.35. In the p-type crystal H102 of this series the room temperature resistivity was 10^5 Ωcm. The temperature dependence of the hole concentration (Fig. 5.4) showed that the Fermi level was pinned on shallow B acceptors (level near $E_v+0.3$ eV). The concentration of uncompensated B acceptors was quite low, close to 5×10^{13} cm^{-3}, which explains the high resistivity of the sample. At the moment it is not

clear what determines whether the Fermi level in semi-insulating p-type samples similar to samples H102 or H128 is pinned by shallow boron acceptors at E_v+0.3 eV or by boron-related D-centers at E_v+0.6 eV. It could be related to the degree of compensation of shallow boron acceptors by nitrogen and other donors.

As mentioned in the previous section, the nitrogen concentration in on-axis samples was consistently lower than in off-axis samples. As a result it was more common to obtain p-type conductivity in such samples. For example, all on-axis samples of series I were p-type with the Fermi level pinned by shallow boron acceptors. Fig. 5.4 shows the temperature dependence of the hole concentration for one such sample (H86). It can be seen that the concentration of uncompensated boron acceptors determined from the saturation region in the temperature dependence is close to the value expected from the nitrogen and boron concentrations measured by SIMS. These results suggest that the conductivity type and resistivity of 6H-SiC crystals grown by HCVD are mostly determined by the concentrations of residual nitrogen and boron and are governed by the effective C/Si ratio via the site-competition effect. The concentration of compensating deep levels in HCVD crystals is not high compared to the concentration of shallow centers. This is confirmed by the results of DLTS and EPR measurements presented in the next section.

5.2 Deep levels measurements.

All n-type samples grown by HCVD contained four major electron traps with apparent activation energies of 0.4 eV, 0.5 eV, 0.65 eV, and 1 eV. Typical DLTS spectra taken on two Si-rich samples grown with the C/Si flow ratios of 0.065 (H127) and 0.12 (H125) are shown in Fig. 5.5. The signatures of the 0.4 eV centers in Fig. 5.5 were quite similar to the signatures of the negative-U 0.4 eV E1/E2 acceptors. The 0.65 eV traps are commonly observed in n-type 6H-SiC crystals and are sometimes referred to as Z1Z2. The 0.5 eV and the 1 eV deep traps were reported to be present in 6H-SiC, but their nature have not been identified.

The 0.4 eV traps are commonly observed dominant centers in n-type HCVD samples. At temperatures close to the 0.4 eV peak in DLTS the 1 MHz capacitance in all samples strongly decreased. In the majority of samples grown with intermediate C/Si flow ratio, the 1 MHz capacitance at temperatures below the 0.4 eV DLTS peak became close to the parasitic capacitance. Under these conditions determination of the concentration of these centers from the standard DLTS procedure was not reliable and instead it was calculated from the difference of concentrations obtained from 1MHz C-V characteristics measured at 300K and at temperature below the DLTS peak (150K temperature). Using

this procedure, the 0.4 eV center concentration in samples H127 and H125 (C/Si flow ratio of 0.065) was found to be 3.5×10^{15} cm^{-3} and 2.6×10^{15} cm^{-3}. For the more C-rich sample H126 (C/Si=0.25) similar estimate gave the concentration of 1.3×10^{15} cm^{-3}. It is notable that these concentrations are reasonably close to those of the 0.27 eV donors determined for the same samples from the Hall effect measurements suggesting that the defects could be related.
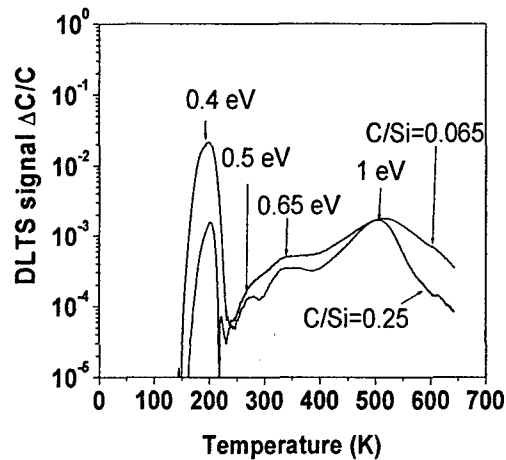

Figure 5.5 DLTS spectra measured on two series IV HCVD n-SiC samples grown with the C/Si flow ratio of 0.065 (sample H127) and 0.12 (sample H125), on miscut substrates; measurements with reverse bias of -5V, forward bias pulse of 1V (50 ms long), and emission rate window of 46.5 s^{-1}

It is instructive to follow the changes in the concentration of different electron traps observed in the series IV samples as the C/Si flow ratio was changing (Fig. 5.6). Though limited to three data points at this time, some general trends are observed. For reference the graph also shows the nitrogen concentration dependence on C/Si ratio (as determined by SIMS). For the 0.27 eV traps, the data were obtained from the temperature dependences of the electron concentration. Concentrations of the 0.4 eV traps were calculated as discussed above. For other traps the concentrations were obtained from DLTS in the standard fashion and include the λ-correction. It can be seen that the density of all traps decreases considerably as the growth mode moves to more C-rich conditions. However, the behavior of different traps is somewhat different in that respect. The changes in the concentration of the 0.5 eV and 0.65 eV traps follow the changes in the nitrogen concentration: corresponding densities decrease with increased

C/Si and then level off. The concentrations of the 0.27 eV (and 0.4 eV) traps and the 1 eV traps decrease monotonically with increasing C/Si flow ratio.
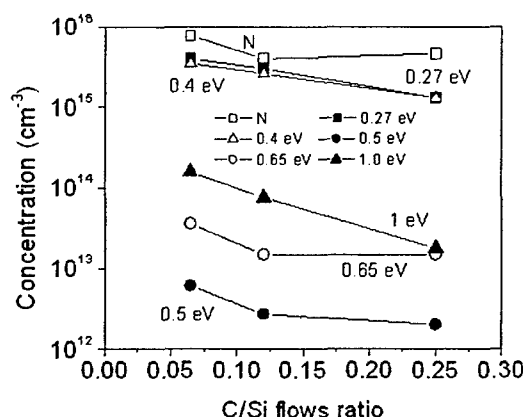

Figure 5.6 Variation of the density of nitrogen (measured by SIMS), the 0.27 eV electron trap, the 0.4 eV trap, the 0.5 eV electron trap, the 0.65 eV electron trap, and the 1 eV electron trap with the C/Si flow ratio in series IV HCVD grown samples prepared on an off-axis substrate.

This difference in behavior for different traps could suggest that the 0.5 eV and the 0.65 eV electron traps involve structural defects whose concentration does not depend on C/Si ratio (a divacancy such as $V_{Si}V_C$). For the Z1/Z2 0.65 eV centers, a similar behavior has been reported for 4H-SiC films grown by standard CVD and has been explained by the assumption that the centers are complexes of nitrogen with structural defects of the $V_{Si}V_C$ type. The 0.27 eV, 0.4 eV, and the 1 eV traps, however, seem to involve defects whose concentration strongly decreases with increasing C/Si ratio, such as C vacancies. The 0.27 eV traps possibly involve nitrogen.

Information about the deep level defects present in the lower half of the bandgap of HCVD-grown SiC is scarce because one can only access the hole traps in Schottky diodes made on n-type films by using optical injection pulses in DLTS measurements. These measurements have not yet been performed. Thus, the only data available are from DLTS measurements on a limited number of p-type samples with the conductivity high enough to allow such measurements. In Fig. 5.7 a spectrum of hole traps is shown for one of the p-type crystals grown on an on-axis 6H-SiC substrate, series I sample H140. The concentration of uncompensated B in this sample was 6×10^{15} cm^{-3}. Hole traps with apparent activation energies of 0.35 eV, 0.6 eV and 0.75 eV can be clearly seen. The 0.6 eV hole traps are most likely the

deep B-related E_v+0.6 eV traps.[21],[22] The 0.35 eV traps are similar to the so called HS1 hole traps observed in DLTS measurements with optical injection performed on n-type SiC films.[23] The concentrations of all these traps decrease with increased C/Si ratio along with a prominent PL band called D1. Such a band was detected in LTPL spectra of HCVD crystals and it's intensity decreased strongly with increasing the C/Si flow ratio (as shown for the series IV samples in Fig. 5.8). Reliable determination of the concentrations of hole traps in Fig. 5.7 could only be done for the 0.75 eV traps (concentration of 10^{13} cm^{-3}) because of the strong series resistance effects and strong freezing out of holes at temperatures below 400K due to the high activation energy of B acceptors.
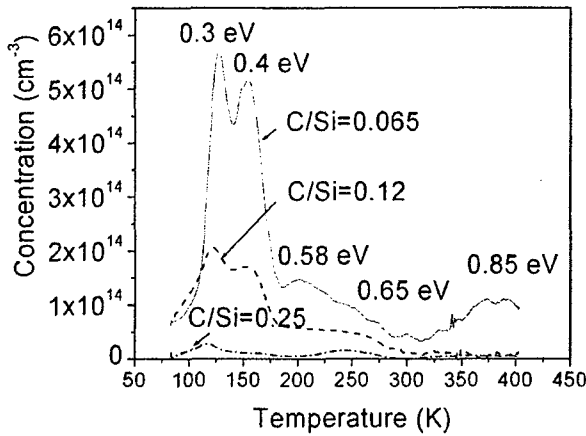
Figure 5.7 DLTS spectrum for one of the HCVD DI -grown p-type samples (H140) obtained with reverse bias of 5V, forward bias of -1V (50 ms long), and emission rate window of 46.5 s^{-1}.
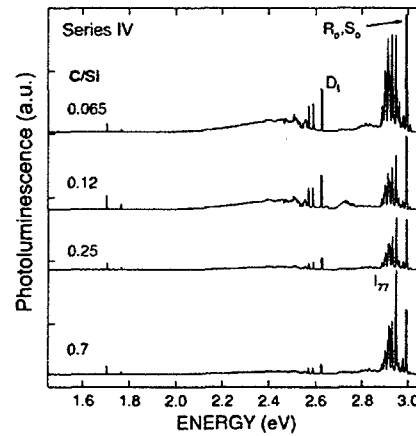
Figure 5.8 LTPL spectra measured showing the luminescence band for four HCVD samples grown with C/Si flow ratios of 0.065, 0.12, 0.25, 0.7 (series IV samples); note the decrease of the DI intensity with increasing C/Si ratio.

5.3 Carrier lifetime measurements

The measurements of carrier lifetimes were performed using Electrom Beam Induced Current method. The basis of the method is explained in Fig. 5.9.
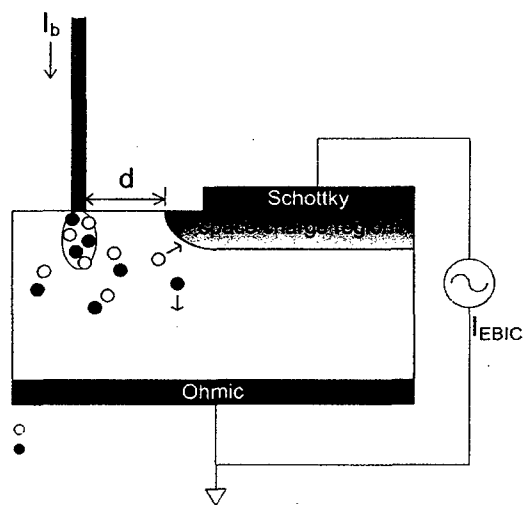
Figure 5.9 Schematic diagram of carrier diffusion length measurement by Electron Beam Induced Current.

EBIC relies on carrier diffusion length measurement using Schottky diode. Stationary electron beam in the SEM (marked as ID in the figure) excites electrons and holes in the semiconductor in the proximity of the diode periphery. The minority carriers diffuse toward the depletion region of the Schottky and the resulting current is detected by an ammeter. Current magnitude ($\ln(I_{EBIC}d^{1.5})$) is plotted as a function of the distance from the diode edge and diffusion length is extracted from the slope (Fig. 5.10).
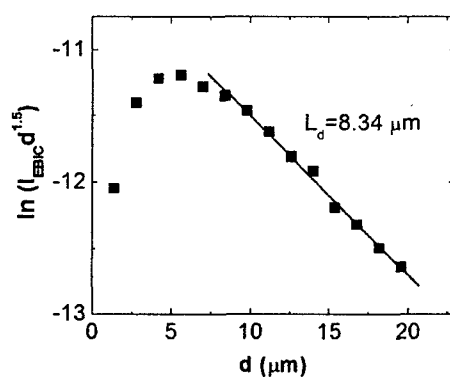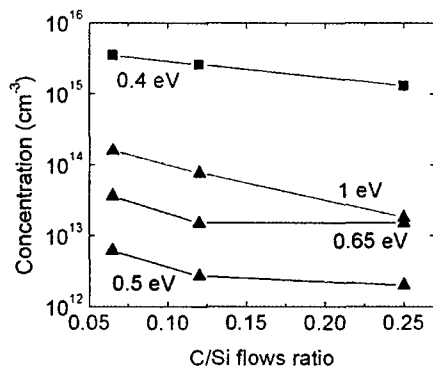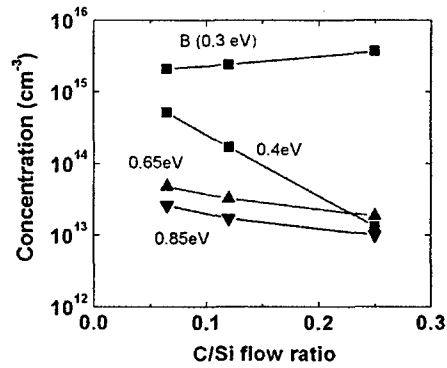

Figure 5.10 Determination of the carrier diffusion length from dependence of EBIC current on distance. Carrier lifetimes have been measured in number of crystals together with deep trap concentrations by DLTS and MCTS. The changes in deep center concentrations versus growth conditions are shown in Fig. 5.11 and 5.12.

(a)　　　　　　　　　　　　　　(b)

Figure 5.11 Deep center concentration in series of HCVD crystals grown at 2050 oC as a function of C/Si ratio. (a) electron traps measured by DLTS, (b) hole traps measured by MCTS.
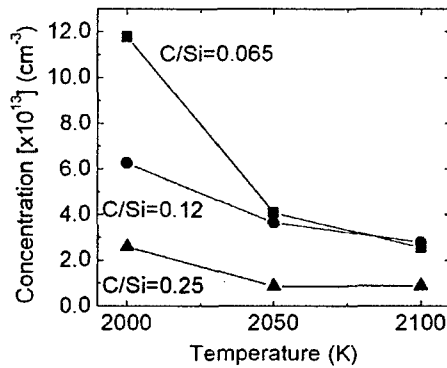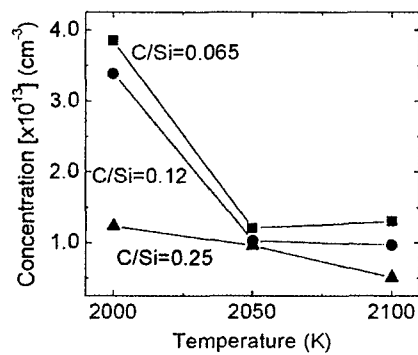

Figure 5.12 Concentration of two major electron traps in Halide CVD crystals measured as a function of C/Si ratio and growth temperature. (a) 0.65 eV trap and (b) 1.0 eV electron trap.

General trends shown in Fig. 5.11 and 5.12 can be summarized as follows: trap concentrations decrease with increasing C/Si ratio and with increasing growth temperature. The same set of crystals have been assessed by EBIC in order to correlate carrier lifetimes with trap concentrations. The results are presented in Fig. 5.13 and 5.14.
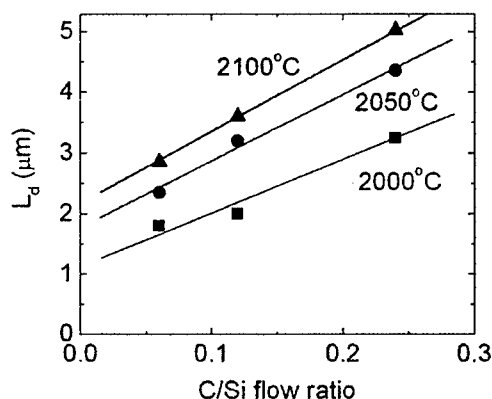
31

Figure 5.13 Carrier diffusion lengths as a function of growth temperature and C/Si ratio.

It is quite apparent that the carrier diffusion lengths correlate very well with the deep trap concentrations as they reflect the two major trends named above. The lifetimes increase both with C/Si ratio and with growth temperature. Since many of the traps observed depend on growth conditions in a similar fashion, it is difficult to equivocally identify the center limiting the lifetimes. However, the best correlation was obtained for the 1.0 eV electron trap (fig. 5.14). At this point, it appears to be the lifetime limiting point defect in Halide CVD crystals. Further experiments are in progress to optimize growth conditions that would give longest possible carrier lifetimes.
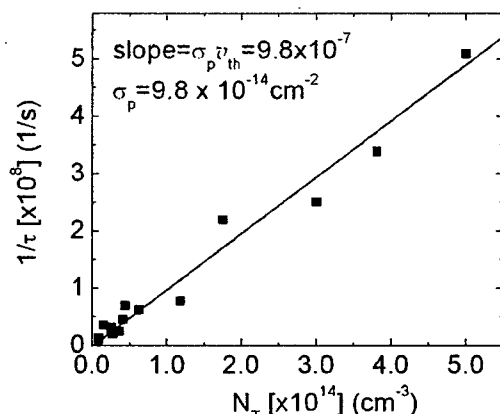

Figure 5.14 Correlation between carrier lifetimes measured by EBIC and concentration of 1.0 eV electron trap.

32

6. Summary

Halide chemical vapor deposition (HCVD) of SiC was used to grow crystals at high growth rates in the 100 μm/hr to 300 μm/hr range. The method allows for control of the gas phase composition by varying the flow rates of the process gases and the growth temperature. There are two regimes for controlling the gas phase composition in HCVD. In the first regime, the local equilibrium between the $C_3H_8 + H_2$ gas mixture and the graphite assembly is achieved. Under these conditions the concentrations of hydrocarbons in the gas phase and, hence, the C/Si ratio can be increased by increasing the hydrogen flow and/or the temperature at the top of the inner injector. The second regime in which the gas phase composition is kinetically controlled is favored by lower temperature of the inner injector and shorter residence time of the $C_3H_8+H_2$ gas mixture. In this regime, the growth rate is controlled by the C3H8 flow into the reaction zone for Si-rich gas phase composition or by the SiCl4 flow into the reaction zone for the C-rich gas phase composition. This regime is similar to the growth in the standard CVD of semiconductor materials and allows accurate variation of the gas phase composition and the growth rate by varying the flows of the Si and C precursors. Changes in the gas phase composition in both the regimes discussed above are expected to affect the incorporation of impurities and deep intrinsic point defect formation.

Nitrogen and boron were identified as the major contaminants in the Halide CVD growth process. Concentrations of other impurities are very low. Incorporation of nitrogen and boron in 6H-SiC crystals follows the behavior reported for 6H-SiC and 4H-SiC films grown by standard silane-based CVD. In particular, nitrogen occupies the C lattice sites and its incorporation is suppressed with increasing C/Si flow ratio. Boron most likely occupies the Si lattice sites and its incorporation is promoted by increasing the C/Si flow ratio. The incorporation efficiency of nitrogen is considerably increased when growing on miscut substrates as compared to on-axis substrates.

The residual nitrogen and boron concentrations in HCVD 6H-SiC crystals are significantly lower than in undoped high purity crystals grown by PVT. This is due to the use of ultra-high-purity precursors and carrier gases and to the possibility to effectively coat the critical parts in the hot zone (the injectors, the susceptor, and the crucible lid to which the seed is attached) with either high-purity pyrolytic graphite formed upon decomposition of propane or by high-purity SiC. The residual nitrogen concentration is also quite comparable with the level achieved in standard epitaxial films grown by silane-based CVD at lower temperatures. The obvious advantage, when comparing CVD and HCVD processes in that respect, is the much higher growth rate in the HCVD process. However, the B contamination level in HCVD-grown

films is much higher than in silane-based CVD films mostly due to the B leaching out from the graphite parts.

In contrast to 4H-SiC films, our studies suggest that a considerable fraction of nitrogen atoms in HCVD-grown 6H-SiC films are paired with native defects of unknown origin formed under Si-rich-growth-conditions. An ionization energy of 0.27 eV was found for this complex from Hall measurements. These centers co-exist with the isolated shallow nitrogen donors with ionization energies of 80 meV and 140 meV and determine the electrical properties in compensated n-type samples. The negative-U acceptor centers with apparent activation energy of 0.4 eV detected by DLTS show behavior similar to the 0.27 eV centers.

Other deep electron traps with activation energies of 0.5 eV, 0.65 eV, and 1 eV all showed a strong decrease in concentration as the C/Si ratio was increased. For the highest C/Si ratios employed in this work the material was still slightly Si-rich, but was very close to stoichiometry based on the fact that the positively charged C vacancies were the dominant centers observed in EPR spectra and that their concentration was very low. The concentrations of traps observed in DLTS in n-type 6H-SiC films grown by HCVD with high C/Si ratios were very low, but still considerably higher than in the best material grown by CVD. The main means of decreasing the concentrations of deep traps could be growth of the films with yet higher C/Si flow ratio and lower concentrations of residual nitrogen.

High-resistivity 6H-SiC crystals grown by HCVD at high C/Si ratios were compensated p-type samples with the Fermi level pinned either near B acceptors or near the B-related deep centers at $E_v+0.6$ eV. The values of resistivity at room temperature were only marginally acceptable for use as semi-insulating substrates in the former case. Also, because in both cases one has to rely on very close compensation of B acceptors by nitrogen donors, these are not easy conditions to achieve for consistently growing semi-insulating material with high yields. It is very desirable to get into the mode in which the concentration of deep centers becomes comparable to the concentration of N and B. For that situation the level of residual contamination should be decreased and growth under more C-rich growth conditions should be mastered (presently, the crystalline quality of the films greatly degrades when too high C/Si flow ratios are employed).

Carrier lifetimes of HCVD material were measured on variety of samples and were found to correlate well with deep center concentrations. Lifetimes increase with increase of C/Si ratio and with increase of

the growth temperature. The center that appears to limit lifetimes is the electron trap located 1.0 eV below conduction band.

References:

1.   Kingon, A.I., et al., J. Am. Cer. Soc. **66**: 558-566 (1983)
2.   Fischman, G.S. and W.T. Petuskey, Journal of the American Ceramic Society. **68**: 185-190 (1985)
3.   Rottner, K. and R. Helbig, Journal of Crystal Growth. **144**: 258-266 (1994)
4.   White, W.B., S.M. Johnson, and G.B. Dantzig, Journal of Chemical Physics. **28**: 751-755 (1958)
5.   Minagawa, S. and H.C. Gatos, Japanese Journal of Applied Physics. **10**: 844-& (1971)
6.   Kordina, O., et al., Appl. Phys. Lett. **69**: 1456-1458 (1996)
7.   Allendorf, M.D. and R.J. Kee, Journal of the Electrochemical Society. **138**: 841-852 (1991)
8.   Clarke, J.T. and B.R. Fox, Journal of Chemical Physics. **46**: 827-& (1967)
9.   Larkin, D.J., et al., Appl. Phys. Lett. **65**: 1659-1661 (1994)
10.   Larkin, D.J., phys. stat. sol. (b). **202**: 305 (1997)
11.   Zhang, J., et al., J. Appl. Phys. **93**: 4708-4714 (2003)
12.   Yamamoto, T., T. Kimoto, and H. Matsunami, Silicon Carbide, Iii-Nitrides and Related Materials, Pts 1 and 2. **264-2**: 111-114 (1998)
13.   Kimoto, T. and H. Matsunami, Journal of Applied Physics. **75**: 850-859 (1994)
14.   Kimoto, T., et al., Journal of Applied Physics. **81**: 3494-3500 (1997)
15.   Henry, A., et al., Applied Physics Letters. **65**: 2457-2459 (1994)
16.   Ivanov, I.G., et al., Journal of Applied Physics. **80**: 3504-3508 (1996)
17.   Glaser, E.R., B.V. Shanabrook, and W.E. Carlos, Applied Physics Letters. **86**: - (2005)
18.   Hemmingsson, C., et al., Journal of Applied Physics. **81**: 6155-6159 (1997)
19.   Hemmingsson, C.G., N.T. Son, and E. Janzen, Applied Physics Letters. **74**: 839-841 (1999)
20.   Hemmingsson, C.G., et al., Physical Review B. **58**: 10119-10122 (1998)
21.   Suttrop, W., G. Pensl, and P. Lanig, Appl. Phys. A. **51**: 231-237 (1990)
22.   Itoh, H., T. Troffer, and G. Pensl, Silicon Carbide, Iii-Nitrides and Related Materials, Pts 1 and 2. **264-2**: 685-688 (1998)
23.   Zhang, A.P., et al., J. Electron. Mater. **32**: 388-394 (2003)